An Adaptive Passive Quasi-Zero-Stiffness Vibration Isolation System through Controllable Lateral Spring Stiffness

Jiale Wang[a],·Liaoyuan Ran[a]·Dunant Halim[a,b,*]·Baiyang Shi[c]·Liang Huang[d]

[a] Department of Mechanical, Materials and Manufacturing Engineering, University of Nottingham Ningbo China, Ningbo, China

[b] Nottingham Ningbo China Beacons of Excellence Research and Innovation Institute, University of Nottingham Ningbo China, Ningbo, China

[c] Department of Engineering Design and Mathematics, University of the West of England, Bristol, UK

[d] Department of Electrical and Electronic Engineering, University of Nottingham Ningbo China, Ningbo, China

*Corresponding author

Abstract

In this work, an adaptive passive quasi-zero-stiffness (QZS) vibration isolation system with controllable lateral springs was proposed and its vibration isolation effectiveness was demonstrated through theoretical and experimental studies. An adaptive passive control strategy was developed to allow for the regulation of the lateral spring length to address the high low-frequency resonant response of the QZS system, while maintaining QZS benefits of increasing the control bandwidth with sufficiently low transmissibility. The effect of the length of the lateral springs on the negative stiffness of the system under static conditions was investigated, and the stability of the system was analyzed to ensure the system's stability during its operation. Through experimental studies, the developed QZS system demonstrated a lower resonant frequency compared to the linear system. Moreover, by employing the adaptive passive control strategy, the dynamic characteristics of the QZS system could be altered from linear to nonlinear through the highly-responsive adjustment of the horizontal spring stiffness. As a result, the excitation of low-frequency resonance could be avoided while simultaneously obtaining an increase control bandwidth with low transmissibility. An experimental test rig utilizing stepper motors to regulate the length of lateral springs was designed and constructed, with the results exhibited a good agreement with the theoretical results. Specifically, experimental results showed that the developed QZS vibration isolation system could effectively cause a reduction of the peaks of vibration response by 26.37% and 69.56% compared to the QZS vibration isolation system without control and a linear isolation system, respectively. The QZS vibration isolation system also achieved an overall reduction in vibration transmissibility with its low-frequency 0-dB bandwidth reduced by 11.8% (from 3.64 Hz to 3.21 Hz) when compared to the linear system, demonstrating the improved vibration isolation effectiveness by varying the spring length at a specified trigger frequency.

Keywords Quasi-zero-stiffness (QZS) vibration isolator · Adaptive passive control · Controllable lateral spring stiffness · Vibration attenuation

1 Introduction

Vibration isolators hold a significant importance for addressing vibration and noise problems in a wide range of engineering applications. Among different types of vibration isolators, a linear vibration isolator is one of the most prevalent and well-developed options to be utilized in practical applications. However, they have a particular drawback, namely, a relatively weak vibration isolation performance in the low-frequency range due to its associated resonance [1], as they typically provide effective vibration isolation only when the excitation frequency surpasses $\sqrt{2}\omega_n$, where ω_n is the system's natural frequency. To optimize the vibration isolation band, engineers commonly adopt a strategy of reducing the stiffness of the supporting springs, thereby decreasing its natural frequency [2]. Accordingly, the development of a vibration isolator with high static stiffness and low dynamic stiffness has become a prominent research focus [3]. A higher static stiffness results in an increased higher static load capacity, while a lower dynamic stiffness enhances the vibration isolation performance. The introduction of nonlinear stiffness elements allows for the realization of quasi-zero stiffness characteristics. Typically, a QZS vibration isolator consists of a vertical spring, which facilitates the load capacity, as well as a novel structure that provides negative stiffness within a limited range. In the static equilibrium position, the negative stiffness generated by the nonlinear negative stiffness structure is counteracted by the positive stiffness provided by the load carrying spring, thus achieving a zero-system stiffness at the static equilibrium position and reduced the dynamic stiffness within a limited dynamic displacement range. Consequently, the system exhibits a lower natural frequency, thereby expanding the isolation bandwidth.

With the study of single-degree-of-freedom (DOF) QZS systems, various types of QZS systems have been developed. Zhou and Ma et al. [3] provided a systematic summary of the research progress and future directions regarding QZS vibration isolators in recent years. The negative stiffness structure of QZS vibration isolators can be generally divided into three parts: the passive, semi-active, and active mechanisms. Among these, the passive mechanism can be further classified into several types, including the mechanical springs, pre-buckled beams, geometrically nonlinear structures, magnetic structures, and composite structures [3]. Alabudzev et al. [4] theoretically studied different types of QZS isolators, including typical QZS systems with a combination of lateral and vertical springs and explored the feasibility of implementation of these systems. Carrella et al. [5,6] and Danh Le et al. [11,12] proposed several typical QZS isolators, which consisted of a vertical spring and two inclined springs mounted on both sides of the mass. Danh Le et al. analyzed their system based on simulation and experimental studies, in which the results showed that this system was effective in improving low frequency vibration performance. Zhao et al. [7-9] used multiple sets of oblique springs to optimize the vibration isolation performance, while Liu et al. [10] designed a QZS isolator with a tunable nonlinear inverter, considering its stability and bifurcation characteristics. Wang et al. [13]. proposed several two DOF QZS isolators, which provided a new direction for the study of QZS vibration isolators, while Liu et al [14] explored the phenomenon of superharmonic vibration in QZS vibration isolators. Several origami structures were also proposed in [15-17], which could effectively suppress low-frequency vibrations by selecting

appropriate system parameters. In [18-20], as inspired by animal/insect limb structures, several biomimetic vibration isolation mechanisms have been proposed with good vibration isolation performances without causing stability problems. Liu et al. [21,22] designed a negative stiffness mechanism using Euler buckled beams, whereas magnetic negative stiffness structures have also been proposed to generate QZS characteristics [23-27]. Although these QZS vibration isolators have been demonstrated to be able to improve the low-frequency vibration isolation performance, they tend to have relatively high low-frequency resonant responses and cannot directly adapt to system's internal and external uncertainties that impact on the vibration isolation effectiveness.

Thus, researchers working have also focused on the development of semi-active and active control mechanisms for QZS vibration isolators. Danh et al. [28] and Palomares et al. [32] designed several isolators with pneumatic negative stiffness structures to control the system stiffness by adjusting the pneumatic actuators. Sun et al. [29] proposed a time-delayed active control strategy, adding a vertical controlled spring and a controller to the traditional three-spring QZS isolator. The peak transmission rate of the isolator could be mitigated through an appropriate adjustment of the delay time, the stiffness of controlling spring and other associated parameters, such as the lateral spring compression and support spring stiffness. Wen et al. [33] presented a new QZS vibration isolator with six oblique springs, and the stiffness of the system was controlled by adjusting the inclination angle of the six inclined springs, although the work focused on the theoretical studies of the system so the practical realization of such a isolator would need further research. In addition, Pu et al. [30] and Zhou et al. [31] proposed several vibration isolation systems with negative stiffness generated by the electromagnetic force between the coil and the magnet, and the stiffness could be adjusted in real time by controlling the current flowing through the coil. Theoretical and experimental results showed that the magnetic negative stiffness structure improved the low-frequency response performance of the vibration isolator. Although using electromagnetic negative stiffness structures for vibration suppression is a desirable direction, these systems are usually more costly and more demanding on sensors/actuators and control algorithms.

Previous research works have indicated that the QZS isolator are more effective than the linear isolators in reducing the natural frequency of the system. However, it is worth noting that for most of the studies their isolation system is generally inclusively attached to the primary mass, so the vibration isolation mechanism and the primary mass altogether experience the excitation. There has been limited research on the vibration isolation mechanisms that are independent to the primary mass. Despite the potential drawback of increased low-frequency vibrations, this arrangement offers the advantage of enhanced adaptability to various isolation targets due to the absence of a negative stiffness mechanism attached to the system's base. As a result, it can exhibit superior robustness, maintaining good control performance even when the mass of the isolation target varies. On the other hand, studies [34,35] have indicated that as the excitation amplitude increases, the traditional QZS systems exhibits an increase in the resonant frequency and the peak amplitude in its transmissibility. Consequently, it can result in an increase in the 0-dB bandwidth of the vibration transmissibility, which is unfavorable for the isolation system especially when dealing with large excitation amplitudes. To address these difficulties, therefore, the proposed QZS system incorporates an adaptive control strategy to transform a linear system into a nonlinear QZS system. The employed adaptive passive control strategy in the proposed QZS system can be used to effectively sustain the low vibration transmissibility within the low-frequency

range. The proposed control system thus simultaneously achieves a reduction in the transmissibility peak amplitude and the widening of the bandwidth. In the present study, the negative stiffness mechanism is designed to be independently attached to the primary mass, enabling its adjustment to suit various isolation requirements. This mechanism encompasses lateral springs who stiffness can be actively adjusted, allowing for precise control over the stiffness of the system. By dynamically varying the stiffness, the proposed control strategy is used to mitigate the large response of the QZS system at low frequencies by detuning its resonance.

This paper is organized as follows. After the introduction in Section 1, Section 2 presents the QZS system, which consists of a vertical spring and two lateral springs with adjustable lengths. Section 3 investigates the dynamic characteristics of the QZS system, comparing it to a linear system with a single degree-of-freedom (DOF). The section provides theoretical analysis on the displacement transmissibility, and subsequently introduces a semi-active control method based on a displacement-feedback adaptive passive control strategy. In Section 4, the focus shifts to the experimental investigation of the proposed control method. Frequency sweep experiments of displacement transmissibility and real-time length adjustment of two lateral springs were conducted to verify the feasibility of the control method. Finally, the paper concludes with Section 6, which presents the key results of the study.

2 Mathematical modeling of the QZS vibration isolation system with controllable lateral springs

2.1. Static analysis of the proposed semi-active QZS isolation system

As in Fig.1, the schematic diagram for the proposed vibration isolation system is presented, which is constructed using one vertical spring and two controllable lateral springs. The lateral springs have the characteristic of variable length, where they are driven by two stepper motors at each side, leading to the controllable spring stiffness. The original un-stretched length of lateral springs is denoted by l_0, and the springs are compressed to the initial length l ($l < l_0$) to achieve QZS characteristics. It is assumed that the mass is in the static equilibrium condition in the vertical direction when $x = 0$.

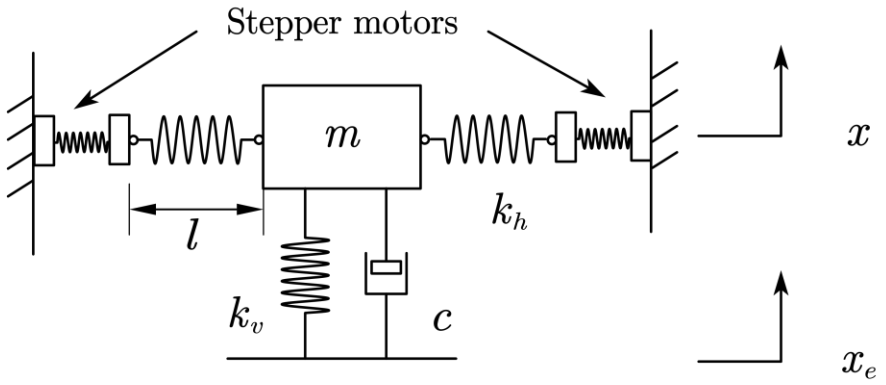

(a)

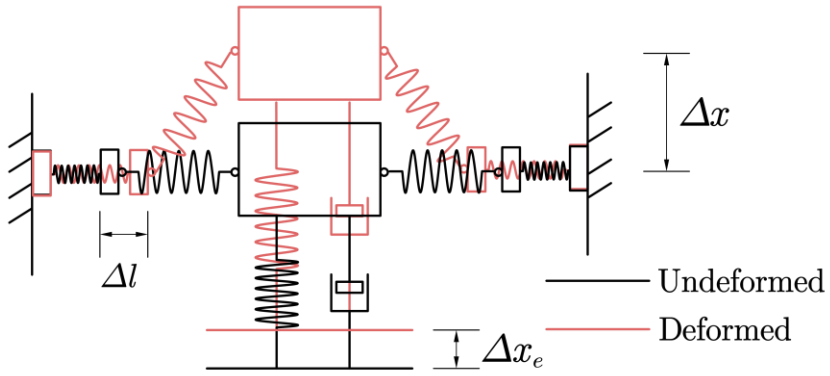

(b)

Fig. 1. A QZS system with controllable lateral springs: The schematic diagrams of (a) the undeformed system and (b) the deformed system with control activated.

It is noted from Fig.1 that the system reaches the static equilibrium, with no externally applied loads. In the equilibrium state, the lateral spring is perpendicular to the vertical spring. The mass undergoes vertical displacement by a distance x, while k_v and k_h represent the stiffness values of the vertical and lateral springs, respectively. The vertical spring connects the base and excitation platform and is characterized by the coefficient of the viscous damping c, while the damping coefficient of the lateral spring is assumed to be negligible. The change in the stiffness of the lateral springs lead to the change in vibration characteristics of the vibration isolation system. Under the static equilibrium state, the equation used to determine the combined downward vertical force f_h, exerted by the two lateral springs on the mass, is as follows:

$$f_h = 2k_h x\left(\frac{l_0}{\sqrt{x^2+l^2}} - 1\right) \tag{1}$$

Therefore, the combined force f acting vertically upward on mass can be obtained as:

$$f = k_v x + 2k_h x\left(1 - \frac{l_0}{\sqrt{x^2+l^2}}\right) \tag{2}$$

By dividing x on both sides of Eq. (2), the stiffness equation of the system is:

$$k = \frac{f}{x} = k_v + 2k_h\left(1 - \frac{l_0}{\sqrt{x^2+l^2}}\right) \tag{3}$$

For the analysis, the equation can be transformed into a dimensionless form. Considering the system's displacement in the static equilibrium state associated with the vertical spring k_v is x_s, with $mg = k_v x_s$, the dimensionless equation can be obtained from Eq. (3) as:

$$F = X + 2KX\left(1 - \frac{U}{\sqrt{X^2 + (UL)^2}}\right) \tag{4}$$

where

$$X = \frac{x}{x_s}, F = \frac{f}{k_v x_s}, U = \frac{l_0}{x_s}, L = \frac{l}{l_0}, K = \frac{k_h}{k_v}. \tag{5}$$

The dimensionless stiffness of the system is:

$$K_t = \frac{F}{X} == \frac{f}{k_v x} \tag{6}$$

It is noted in the aforementioned equation that the system stiffness K_t of the system is affected by several factors. These factors include the original length l_0 of the lateral spring, the controllable length l of the lateral spring, and the stiffness parameters k_v and k_h. By adjusting these parameters, the system stiffness K_t can be changed from positive to negative when the mass displacement X is in a specific small region, which is beneficial for achieving high static-low dynamic stiffness characteristics. Here, U is set to 6.2701 for the following analysis, with Figs. 2 (a) and (b) showing the dimensionless combined force F and stiffness K_t with varying dimensionless X and the compression ratio of lateral spring L, respectively.

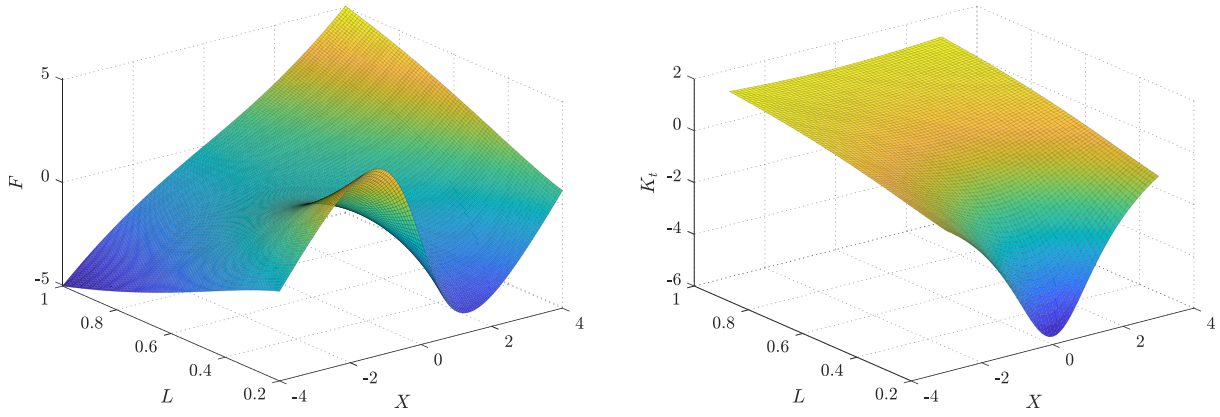

(a) (b)

Fig. 2. The influence of the compression ratio of lateral spring L and the dimensionless system's displacement X on (a) the dimensionless external force F and (b) the dimensionless system's stiffness K_t.

Figure 2 shows a significant shift in the relationship between F and X as L increases. Initially, this relationship exhibits extremely non-linearity and demonstrates a specific range of quasi-zero-stiffness characteristics at a certain range of X. However, with the increase in L, the relationship gradually towards linearity within the displacement range

of the system. It is worth noting that when $L = 1$, the system does exhibit the characteristics of a single DOF linear system. However, although the system closely approximates linearity, the effect of the lateral spring cannot be disregarded. This is evident in Fig. 2 (a), where the force-displacement curve of the system deviates from linearity when $L = 1$, so it is important to account for the nonlinear effects introduced by the lateral spring. From, Fig. 2 (b), it can be observed that as X approaches to zero, a decrease in L leads to a reduction in k. Furthermore, the influence of X on K_t diminishes with increasing L with the system's displacement range. Therefore, by altering l of the lateral spring, it is possible to manipulate the system's stiffness, thereby offering a potential for vibration mitigation. The force-displacement curves with varying stiffness ratio K is plotted in Fig. 3.

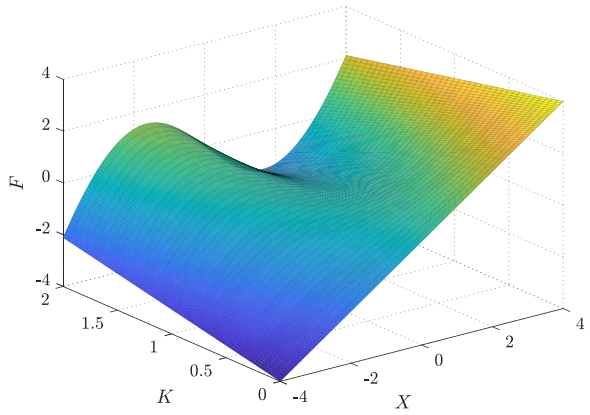

Fig. 3. The influence of the dimensionless system's displacement X and stiffness ratio K on the external force F.

It is evident that the stiffness ratio K and the compression degree L of the lateral spring jointly determine the QZS characteristics of the isolation system. A higher stiffness ratio K results in more the more pronounced nonlinear characteristics within the system, while a lower stiffness ratio K brings the system is closer to linearity. When the stiffness ratio K approaches to zero, it corresponds to a linear system in which the lateral springs at both ends are absent, so in this case, the system can be considered as a single DOF linear system. The effect of the compression degree L of the lateral spring on the nonlinear characteristics of the system is observed to be similar to the stiffness ratio K. In particular, when the compression degree is larger, L is smaller, and the nonlinear characteristic of the system is more obvious.

2.2 Stability analysis

Here, the stability analysis of the proposed vibration isolation system is undertaken to ensure the stability of the system under varying controllable spring stiffness settings. It has been previously shown in the present work that a significant influence of lateral spring length l and spring stiffness are critical parameters that influence nonlinear characteristics of the vibration isolation system. An improper selection of the spring stiffness and spring length l can lead to an unstable QZS system, posing potential risks in its applications. Ensuring stability necessitates that the equilibrium position of the system, the spring stiffness ratio K, along with other parameters need to be kept within a

reasonable range. When the system is in a static equilibrium state, neglecting the damping term, the combined force applied to the system $F = 0$ can be approximated using third-order and fifth-order Taylor expansion of Eq. (5), yielding the following results:

$$F = \alpha X + \gamma_1 X^3 = 0 \ \text{(3rd order)} \tag{7}$$

$$F = \alpha X + \gamma_1 X^3 - \gamma_2 X^5 = 0 \ \text{(5th order)} \tag{8}$$

where $\alpha = 1 - 2K(1-L)/L$， $\gamma_1 = \frac{K}{U^2 L^3}, \gamma_2 = \frac{K}{U^4 L^5}$, while it is important to note that, as $K > 0, L > 0 \ and \ U > 0$, $\gamma_1 > 0$ and $\gamma_2 > 0$.

The solution to Eq. (8) gives：

$$X_1 = 0 \tag{9}$$

$$X_2 = -\sqrt{\frac{\gamma_1 + \sqrt{{\gamma_1}^2 + 4\alpha\gamma_2}}{2\gamma_2}} \tag{10}$$

$$X_3 = \sqrt{\frac{\gamma_1 - \sqrt{{\gamma_1}^2 + 4\alpha\gamma_2}}{2\gamma_2}} \tag{11}$$

$$X_4 = -\sqrt{\frac{\gamma_1 - \sqrt{{\gamma_1}^2 + 4\alpha\gamma_2}}{2\gamma_2}} \tag{12}$$

$$X_5 = \sqrt{\frac{\gamma_1 + \sqrt{{\gamma_1}^2 + 4\alpha\gamma_2}}{2\gamma_2}} \tag{13}$$

The above solutions can yield three different stability cases:

- Case 1: ${\gamma_1}^2 + 4\alpha\gamma_2 < 0$. In this case, there exists only one solution, $X_1 = 0$.
- Case 2, ${\gamma_1}^2 + 4\alpha\gamma_2 > 0, \gamma_1 - \sqrt{{\gamma_1}^2 + 4\alpha\gamma_2} < 0$ & $\gamma_1 + \sqrt{{\gamma_1}^2 + 4\alpha\gamma_2} > 0$. In this case, the equation will yield three distinct solutions, namely $X_1, X_2 \ and \ X_5$. It is noted that the condition ${\gamma_1}^2 + 4\alpha\gamma_2 > 0$ ensures the existence of these solution, as both γ_1 and $\gamma_2 > 0$.
- Case 3, ${\gamma_1}^2 + 4\alpha\gamma_2 > 0$, $\gamma_1 - \sqrt{{\gamma_1}^2 + 4\alpha\gamma_2} > 0$, where all five solutions exist.

It summary, firstly, when $\alpha < 0$ and $\gamma_1 < \sqrt{-4\alpha\gamma_2}$, the system only has one equilibrium point. Secondly, when $\alpha > 0$, the system has three equilibrium points. Finally, when $\alpha < 0$ and $\gamma_1 > \sqrt{-4\alpha\gamma_2}$, the system has five equilibrium points. Figure 6 shows the stability region based on these three different cases.

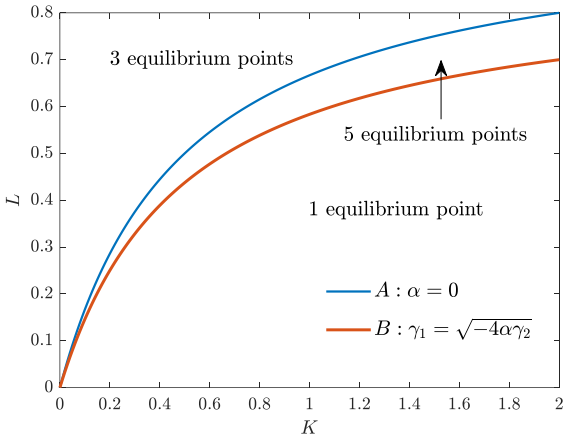

Fig. 4. Stability regions for the QZS vibration isolator.

The relationship between the equilibrium points and the stability region of the system can be observed in Fig. 4. This figure indicates how the equilibrium points are categorized by two discriminant lines, namely line A corresponding to $\alpha = 0$ and line B corresponding to $\gamma_1 = \sqrt{-4\alpha\gamma_2}$. By adjusting the characteristic values of K and L of the system, the number of equilibrium points can be modified, noting that when the system possesses more than one equilibrium point, the system will tend to become unstable so this should be avoided. To further investigate the effect of the number of equilibrium points on system stability, consider the potential energy function V of the system defined as:

$$V = \frac{1}{2}\alpha X^2 + \frac{1}{4}\gamma_1 X^4 - \frac{1}{6}\gamma_2 X^6 \tag{15}$$

By setting K and L to different values, Fig. 5 can then be plotted.

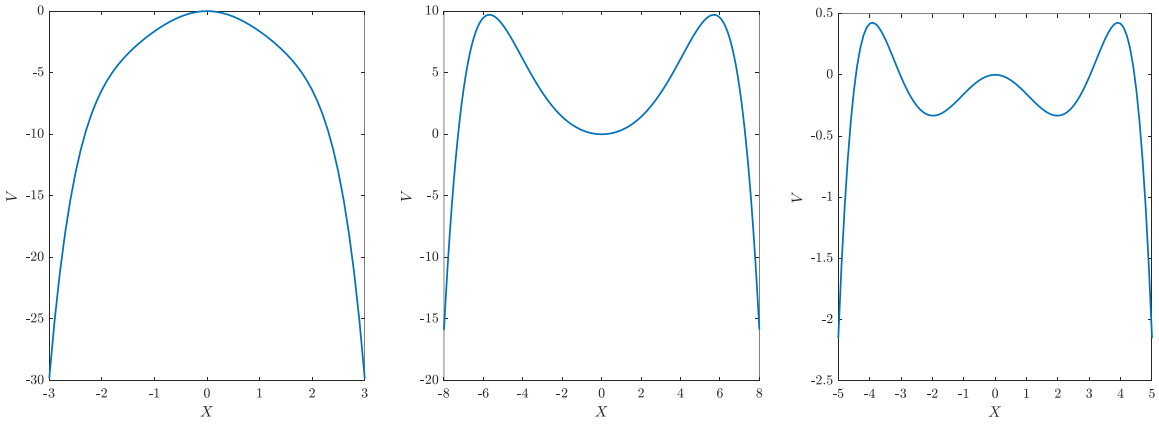

(a) (b) (c)

Fig. 5. The potential energy function for the QZS vibration isolation system when (a) $K = 1$ and $L = 0.3$; (b) $K = 0.4$ and $L = 0.7$; and (c) $K = 1.6$ and $L = 0.7$

As depicted in Fig. 5, three distinct scenarios regarding the number of equilibrium points are observed when K and L are fixed at different values to the potential energy function. In Fig. 5 (a), the potential function V exhibits a solitary trap, indicating the presence of a single equilibrium point. Conversely, Fig. 5 (b) shows the emergence of two additional traps in the potential function curve, suggesting a relatively less stable system configuration. Figure 5 (c) represents a potential function with five traps, implying the presence of five equilibrium points. This configuration implies a higher level of instability within the system. In practice, to ensure the operational safety and potential instability, the spring length and stiffness of the QZS system therefore need to be regulated to be within the region of Case 1.

3. Dynamic characteristics of the QZS system with controllable lateral springs

3.1 Governing equations of the linear and QZS systems

In this work, a comparative analysis on dynamics characteristics between the linear system and QZS system are conducted, specifically by examining their frequency response and displacement transmissibility characteristics. For a single DOF linear system, the lateral springs at both ends exerts zero force to the mass, and the equation of motion of the system can be obtained as:

$$m\ddot{x} + c\dot{x} + k_v x = c\dot{x_e} + k_v x_e \tag{16}$$

Letting $x(t) = X_m cos\omega t, x_e(t) = X_e cos(\omega t + \theta)$ in Eq. (16):

$$(-m\omega^2 X_m + k_v X_m)^2 + (c\omega X_m)^2 = (c^2\omega^2 + k_v^2)X_e^2 \tag{17}$$

Based on Eq. (17), it can be seen that the frequency response curve of the linear system is mainly affected by factors such as damping, vertical stiffness, and the external excitation. Additionally, the displacement transmissibility of the system can be readily derived from the frequency response of the system. Let the displacement transmissibility be $T_{d.i} = \frac{X_m}{X_e}$:

$$T_{d.i} = \sqrt{\frac{(c^2\omega^2 + k_v^2)}{(-m\omega^2 + k_v)^2 + (c\omega)^2}} \tag{18}$$

Similar to the linear system, the governing equation of the QZS system can be expressed according to Eq. (3) and Eq. (15) as:

$$m\ddot{x} + c\dot{x} + k_v x + 2k_h x\left(1 - \frac{l_0}{\sqrt{x^2 + l^2}}\right) = c\dot{x_e} + k_v x_e \tag{19}$$

To simplify the calculation, the governing equation of the QZS system are expanded in the 3rd and 5th orders using Taylor expansion, respectively:

$$m\ddot{x} + c\dot{x} + \alpha x + \gamma_1 x^3 = c\dot{x_e} + k_v x_e \tag{20}$$

$$m\ddot{x} + c\dot{x} + \alpha x + \gamma_1 x^3 - \gamma_2 x^5 = c\dot{x_e} + k_v x_e \tag{21}$$

where $\alpha = k_v + 2k_h(1 - l_0/l)$, $\gamma_1 = k_h l_0/l^3, \gamma_2 = k_h l_0/l^5$.

The force-displacement curves obtained from Eqs. (18)-(20) are compared as shown in Fig. 6. The original function and the two functions after the Taylor expansion fit well with the nonlinear stiffness characteristic of the QZS system. Through comparing three functions, it is found that the disparities between the Taylor expansion function and the original function are negligible within the range of small mass displacement. Considering the proposed control strategy focused on the range of mass displacement satisfying the zero-stiffness characteristic, the present work uses a third-order Taylor expansion in the subsequent analysis.

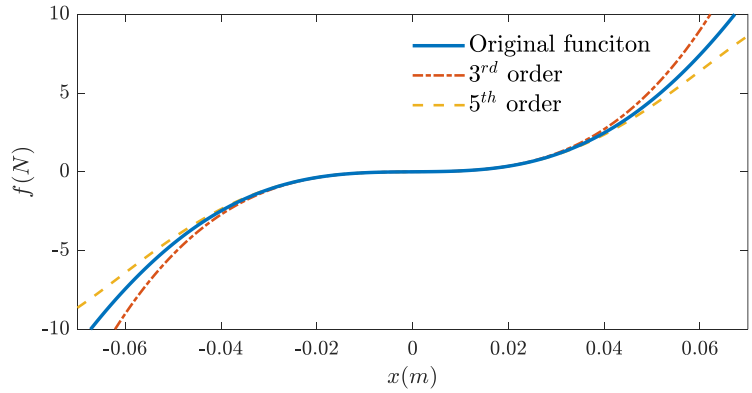

Fig. 6. A comparison of the original function and the functions after Taylor cubic and quintuple expansions.

3.2 Frequency response function and displacement transmissibility of the QZS with/without adaptive control

After Taylor expansion, the harmonic balance method is used to obtain the frequency-domain solution of Eq. (19). By introducing $x(t) = X_m cos\omega t, x_e(t) = X_e cos(\omega t + \theta)$, Eq. (20) can be expressed by:

$$-m\omega^2 X_m + \alpha X_m + \frac{3}{4}\gamma X_m^3 = -c\omega X_e sin\theta + k_v X_e cos\theta \tag{22}$$

$$c\omega X = c\omega X_e cos\theta + k_v X_e sin\theta \tag{23}$$

By squaring Eq. (22) and Eq. (23) and adding them together, the following can be obtained:

$$\left(-m\omega^2 X_m + \alpha X_m + \frac{3}{4}\gamma X_m^3\right)^2 + (c\omega X_m)^2 = (c^2\omega^2 + k_v^2)X_e^2 \tag{23}$$

The displacement transmissibility is expressed by $T_{d.i} = \frac{X_m}{X_e}$:

$$T_{d.i} = \frac{X_m}{\sqrt{\frac{\left(-m\omega^2 X_m + \alpha X_m + \frac{3}{4}\gamma X_m^3\right)^2 + (c\omega X_m)^2}{(c^2\omega^2 + k_v^2)}}} \tag{24}$$

By assigning a typical value to the QZS system used in the following experimental setup, as presented in Table 1, Fig. 10 depicts the displacement transmissibility of the system with varying lateral spring length and the fixed vertical spring stiffness $k_h = 318N/m$, as well as the system with the varying lateral spring stiffness k_h with fixed $l = 0.111\ m$.

Table 1 Parameter values used in the experimental QZS system.

$k_v\ (N/m)$	$k_h(N/m)$	$m\ (\mathrm{Kg})$	$l(m)$	$l_0(m)$	c
380	318	1.094	0.120-0.177	0.177	3.251

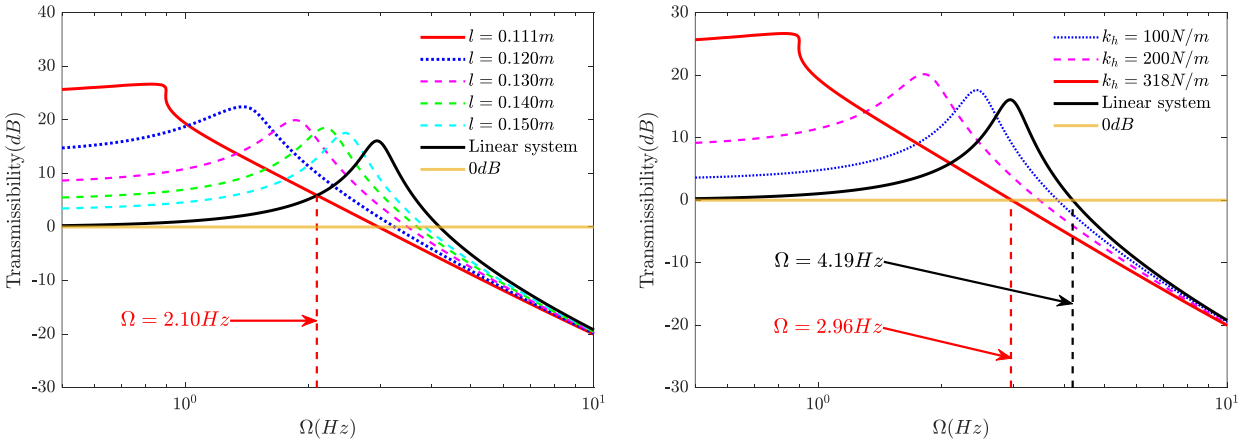

(a) (b)

Fig. 7. The displacement transmissibility comparison of linear and QZS systems for (a) varying l and (b) k_h when $l = 111mm$.

As shown in Fig.7 (a), when comparing the QZS system with the linear system, it is observed that the QZS system has a lower resonant frequency. Additionally, as the length of the lateral spring l decreases, the nonlinear characteristics of the system become more obvious particularly at the resonance region. The lower resonant frequency and the larger resonant peak of the QZS system might render it unstable for sufficiently low frequency vibrations. The QZS system indeed reduces the resonant frequency compared to the linear system. However, in response to sufficiently low frequency vibration, particularly in proximity to the resonance of the QZS system, the QZS system will significantly amplify such excitation. This phenomenon could have a substantial impact on the operation of the vibration isolation system, so this will be addressed with the proposed adaptive passive control strategy. Figure 7 (b) shows that the variation in the lateral spring stiffness k_h results in a similar phenomenon to those observed when adjusting the length

of the lateral spring. Specifically, an increase in k_h lead to an alteration in the resonant frequency that increases the transmissibility within the low-frequency range of the vibration isolation system. Therefore, both excessively low and high lateral spring stiffnesses are generally not desirable to improve the vibration isolation performance of the system. It is important to note that further actuating the lateral spring length can only result in a proportional increase in the spring stiffness. Should the value of k_h be relatively large, this can may induce a substantial increase in the low-frequency vibration amplitude, thereby rendering the system impractical. Conversely, if k_h is relatively small, although the vibration amplitude within the low-frequency range might be minimal, the resulting shift in the natural frequency might not be significant enough to effectively improve the control bandwidth with low transmissibility through control. Therefore, the selection of the k_h is essential for the control strategy and need to be carefully considered.

In order to widen the control bandwidth with low transmissibility while reducing the resonant responses, enabling the effective operation of the vibration isolation system, an adaptive passive control method is proposed. The control loop's block diagram for the QZS system, featuring controllable spring stiffness, is shown below in Fig. 8.

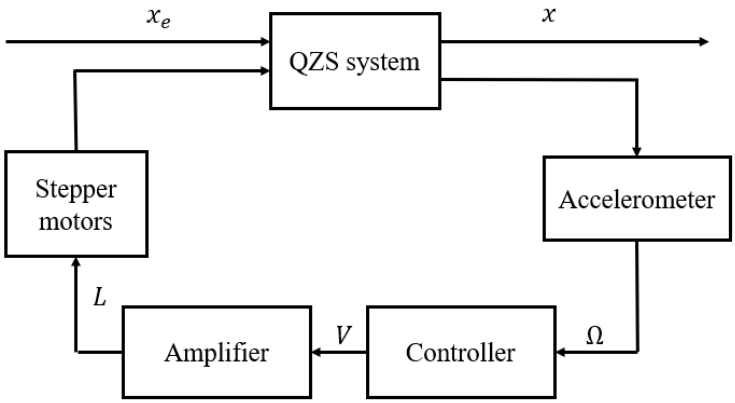

Fig. 8. A block diagram of the adaptive passive control strategy.

The controllable spring length L is adjusted in the QZS system through the utilization of stepper motors. Real-time excitation frequency data is collected by the accelerometer, which enables the controller to generate digital voltage signal to the stepper motors. This process enables the regulation of desired spring length L for the lateral springs, consequently varying the spring stiffness accordingly. Figure 12 illustrates the control principle, which implements the adaptive passive control strategy to enhance the vibration isolation performance by selectively adjusting the length of the lateral springs.

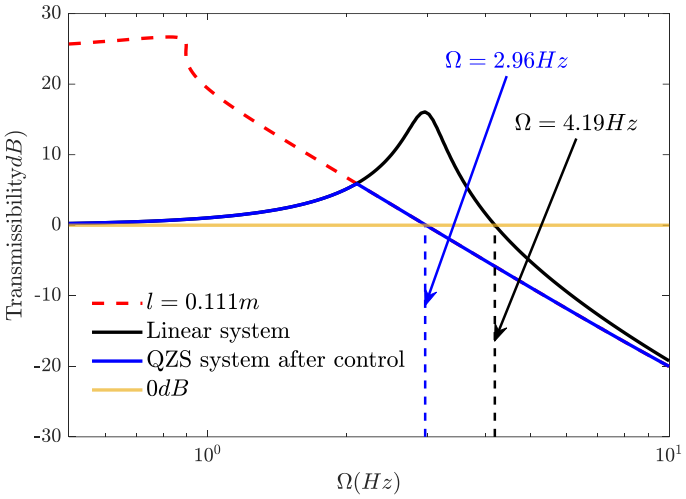

Fig. 9. The displacement transmissibility of QZS system with/without applying adaptive control.

Based on Fig. 9, it evident that the displacement transmissibility curves for QZS system with spring length $l = 0.111\ m$ and linear system exhibits intersection points with 0-dB baseline. The magnitude of frequency at this point is approximately 2.10 Hz, referred to as the trigger frequency Ω_T. Below this trigger frequency, the vibration amplitude of QZS system is significantly higher than that of linear system. However, above 2.10 Hz, the vibration frequency of linear system becomes significantly greater than that of QZS system. The control methodology aims to regulate the length of l based on the detected primary vibration frequency. Specifically, for higher vibration frequencies (e.g., above 2.10 Hz), a shorter length l of 0.111 m is chosen, while for lower vibration frequencies (e.g., below 2.10 Hz), the original spring length l of 0.177 m is selected. By implementing this approach, the system effectively avoids the significant resonant peak across the entire frequency range, leading to a sustained low vibration transmissibility. By appropriately adjusting the length of the lateral spring, the vibration isolation performance of the QZS system can be significantly enhanced, resulting in a 0-dB bandwidth decrease from 4.19 Hz to 2.96 Hz, and the respective reduction of vibration peaks of 77.53% and 65.50%, from 26.22 dB to 5.89 dB and 17.07 dB to 5.89 dB, compared to QZS system without control and linear system, respectively. The corresponding resonant frequency is decreased from 2.96 Hz to 2.10 Hz after the control. This adaptive passive control strategy does not only reduce the resonant frequency but also diminishes the vibration amplitude due to the resonance, while the transmissibility can be kept lower in the low-frequency range.

4. Experimental verification of the QZS system with/without control

In the preceding section, the QZS system's approximated combined force is represented through the utilization of a Taylor series expansion. Additionally, the harmonic balance method is employed to evaluate the frequency response function characteristics and displacement transmissibility of the QZS system. In this section, an experiment test rig was established to verify the proposed theoretical results and assess the performance of the control mechanism for the QZS system under displacement excitation as shown in Fig. 10. The sweep analysis of the displacement transmissibility

was conducted by varying the spring length l, and the effectiveness of the adaptive control method was evaluated. Simultaneously, real-time measurements at different fixed frequencies of the QZS system's response were recorded to further analyze its dynamic behavior.

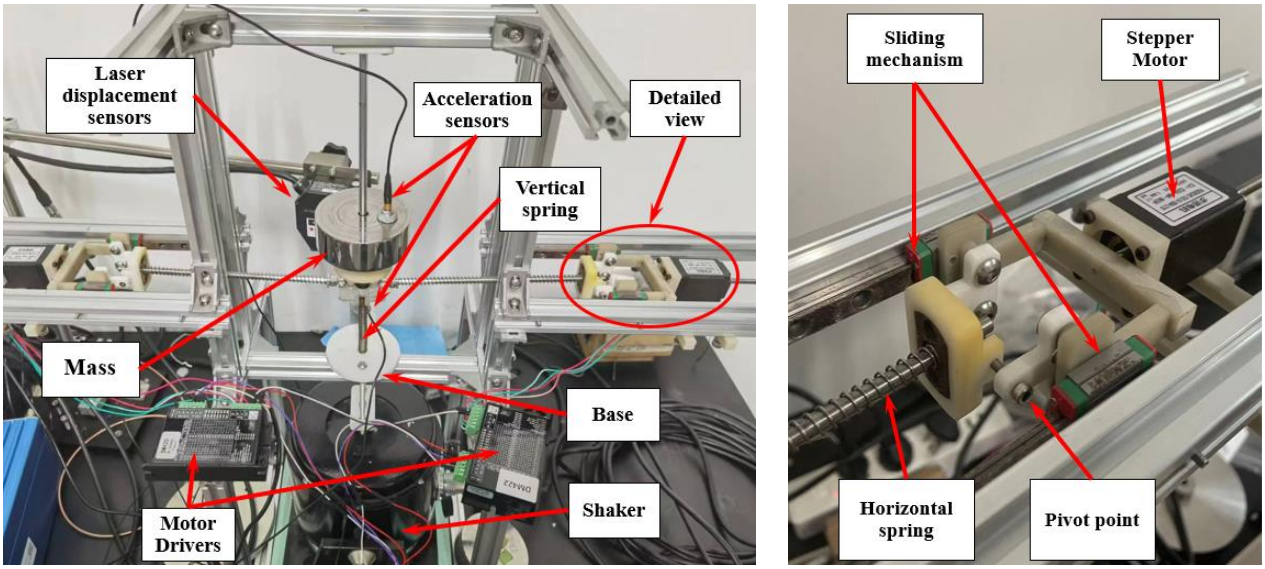

(a) (b)

Fig. 10. (a) An experimental set up of the QZS system with controllable lateral springs. (b) A detailed view of actuation mechanism.

The electrodynamic shaker, positioned at the base, was utilized to generate displacement excitation between the mass and the foundation through the connection of vertical spring. A signal generator was integrated to the shaker, which was utilized to generate the sweep sinusoidal signal, and the minimum excitation frequency of the shaker was 1 Hz. The system's damping was determined through experimental modal hammer testing, in which the logarithmic decay rate was used to calculate the experimental damping ratio. The data acquisition and control unit employed in this set up comprised of a comprehensive set of equipment from national instruments (NI), encompassing multi-functional modules. The accelerometers installed at the mass and base were YMC261A05 models, featuring a sensitivity of 2.0 pC/g. The displacement sensors (Keyence LH-H050) were used measure the mass displacement at specific low frequencies to ensure the measurement accuracy. To monitor the real-time variation in the length of the lateral spring, the input to the stepper motors in the form of Pulse Width Modulation wave (PWM) was recorded. The original voltage signal from the sensors was collected by the NI acquisition cards and sent to the computer using LabVIEW software. Each response amplitude and frequency necessary for calculating the displacement transmissibility was obtained by applying the Fast Fourier Transform (FFT) to a specific time period, based on the set sampling frequency.

For the implementation of adaptive passive control, two stepper motors were mounted on the steel beams at both sides of the system. The stepper motor screw was connected to a push rod, which was further linked to the T-shaped aluminum frame. The T-shaped connecting member was secured onto the slider, enabling the stepper motors to drive the slider inward or outward as desired. For the adaptive control process, the measurement frequency was compared

with the trigger frequency Ω_T set by adaptive passive control strategy to decide whether the stepper motors moved inward or outward.

5. Experimental results and discussion

5.1 Displacement transmissibility of the QZS system with varying spring length

The displacement transmissibility of the QZS system with varying spring length l, were numerically solved by the Runge-Kutta method and compared with the theoretical results of displacement transmissibility curves. The analytical, numerical, and experimental displacement transmissibility curves under the same excitation displacement amplitude of 1.5 mm with l=120 mm, 130 mm, 140 mm and 150 mm, are compared in Fig. 11.

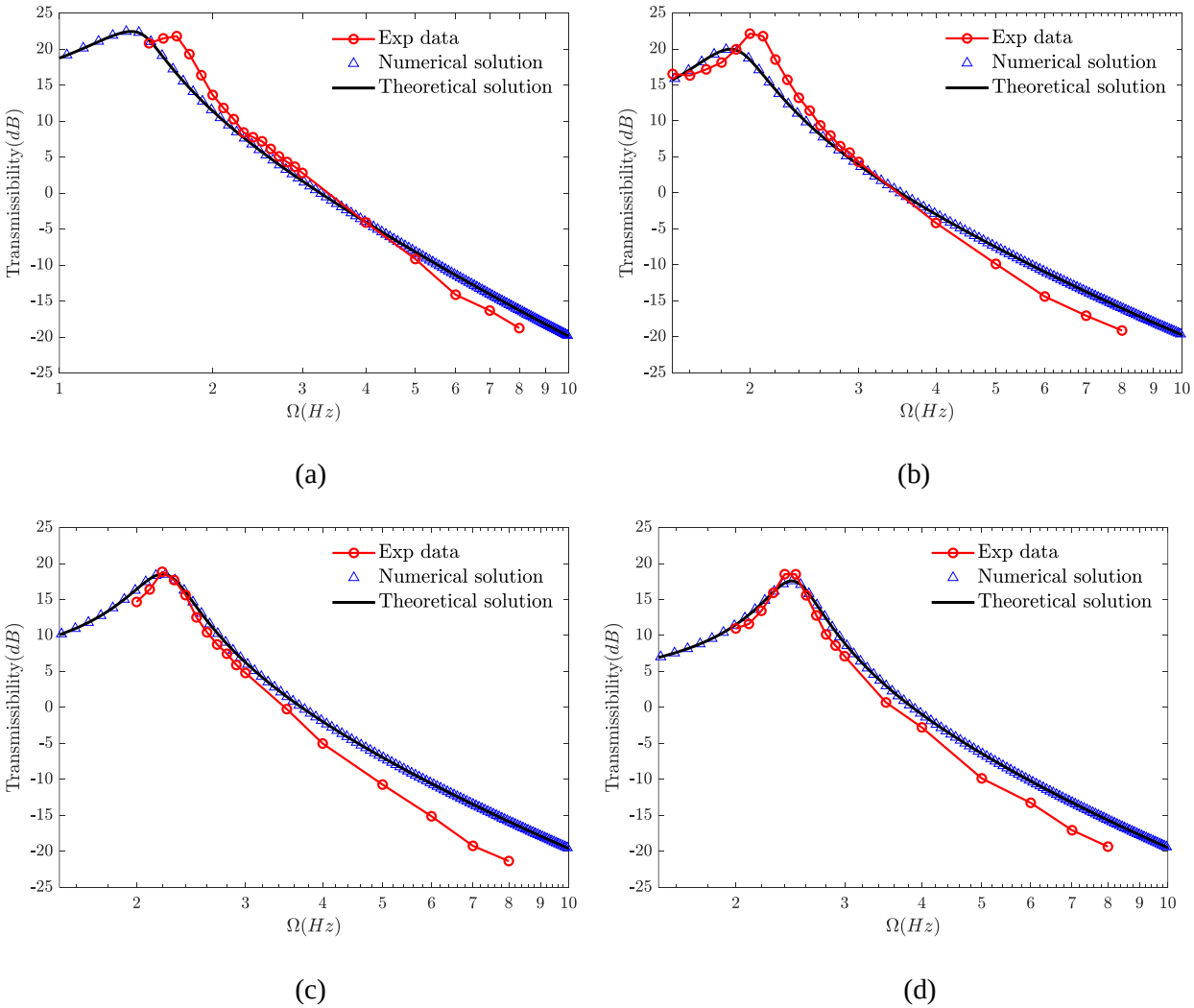

Fig. 11. Displacement transmissibility: (a) $l = 120$ mm, (b) $l = 130$ mm, (c) $l = 140$ mm, (d) $l = 150$ mm, with the excitation displacement amplitude of 1.5mm.

As shown in Fig.11, as the length l of the lateral spring decreased, the resonant frequency of QZS progressively shifted towards lower frequencies. In order to widen the bandwidth for effective vibration isolation, it is necessary to choose a smaller value of l, thereby reducing the resonant frequency and subsequently increasing the resonant peak of

the system. It can be also observed that the numerical and experimental results closely aligned with the theoretical results across the majority of frequency intervals. The experimental results demonstrated an excellent agreement with the theoretical results, reflecting the accuracy of theoretical equations.

5.2 Displacement transmissibility of the QZS system with adaptive control strategy

Initially, the stepper motors were reset to its original position l_i before the start of the testing. Subsequently, a while loop was implemented to facilitate real-time input and output signals, with a shift register used within the while loop to record the instantaneous position of the stepper motors. The collected excitation frequency ω was compared against the trigger frequency Ω_T and the springs length was actuated to the desired spring length l_d if the measured frequency fell outside the designated range. The following chart of the control strategy is represented, as shown in Fig. 12.

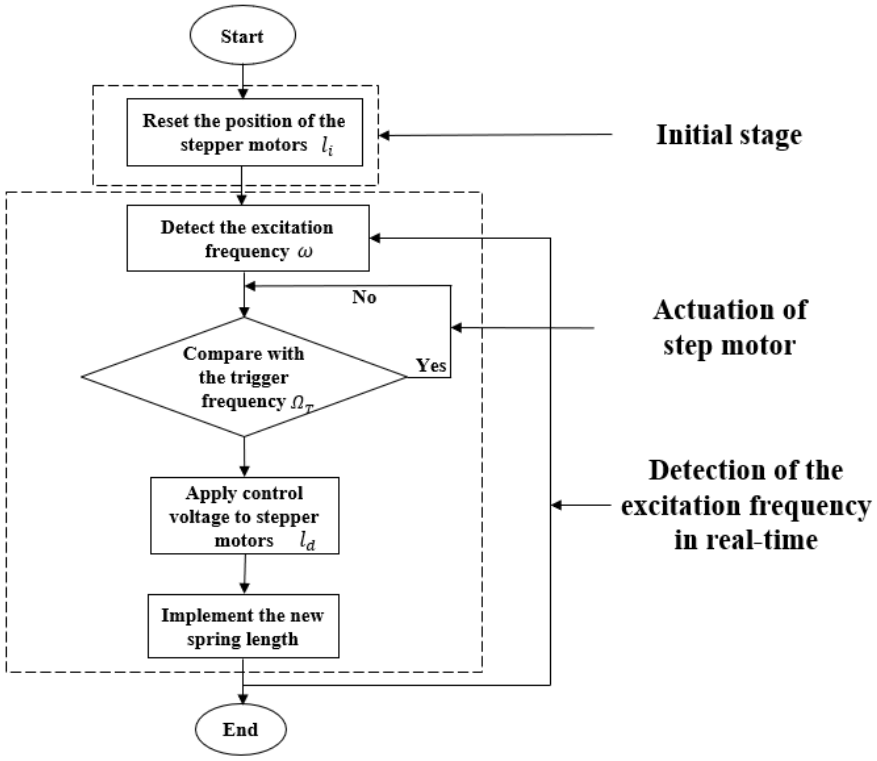

Fig. 12. The flow chart of the adaptive control strategy.

In the experiment set up, the stepper motor capacity posed a limitation on shortening the spring to 111mm, so the target spring length was set at 120 mm instead. Additionally, a trigger frequency of 2.30 Hz was specified, so when the detected frequency exceeded 2.30 Hz, the stepper motors would be activated to adjust the spring length to the desired value of 120 mm. Conversely, if the detected frequency was equal to or lower than 2.30 Hz, the spring length would remain unchanged at its original position. Figure 13 shows the experimental results of the QZS system with adaptive control strategy and the linear system without control by exciting a frequency sweep signal from 1.5 Hz to 8 Hz.

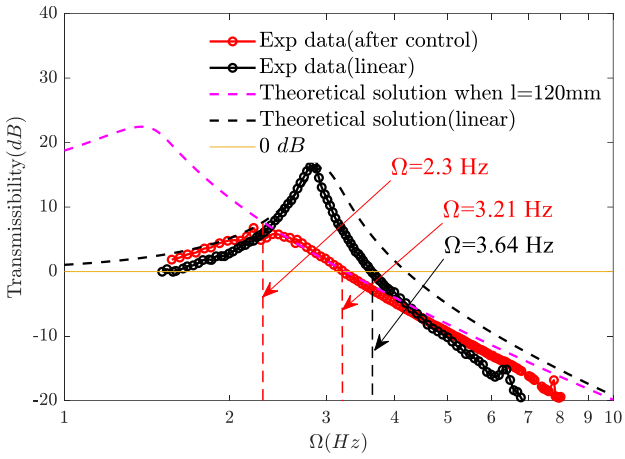

Fig. 13. Frequency-domain displacement transmissibility using the adaptive passive control.

As shown in Fig.13, the experimental results show a consistency with the corresponding theoretical results. The implementation of the adaptive passive control strategy resulted in significant reductions in the vibration peak of the system. Specifically, compared to the QZS system without control (with a spring length of 120 mm), the vibration peak was reduced by 26.37%, decreasing from 22.41 dB to 6.82 dB. In comparison, the vibration peak of the linear system was reduced by 69.56%, decreasing from 16.50 dB to 6.82 dB. The 0-dB bandwidth of the proposed QZS isolation is decreased by 11.81% from 3.64 Hz to 3.21 Hz so to achieve a lower transmissibility at low frequencies. These results demonstrated the effectiveness of the adaptive passive control strategy in minimizing vibration amplitudes for both systems. A slight deviation was observed at an approximate frequency of 2.30 Hz, which could be accounted for by the transient responses resulting from the motion of the stepper motors. As the stepper motors were unable to instantaneously adjust the spring length from 177 mm to 120 mm, the abrupt variation in the lateral spring stiffness led to a slight discrepancy in the magnitude of the displacement transmissibility. As predicted in Section 3.2, the vibration suppression bandwidth and peak amplitude of the adaptive passive QZS vibration isolator has been increased compared with the linear system.

5.3 Time responses of the QZS system with varying l-length at different excitation frequencies

To investigate the dynamic response of the QZS system under varying excitation frequencies, a series of experiments were conducted. Excitation frequencies of 2.1 Hz, 2.5 Hz, 3 Hz, and 4 Hz were used, with the variation of the spring length from 155 mm, 140 mm, 130mm and 120 mm. To observe the relationship between spring length and time, the PWM signal applied to the stepper motors is plotted in Fig. 14.

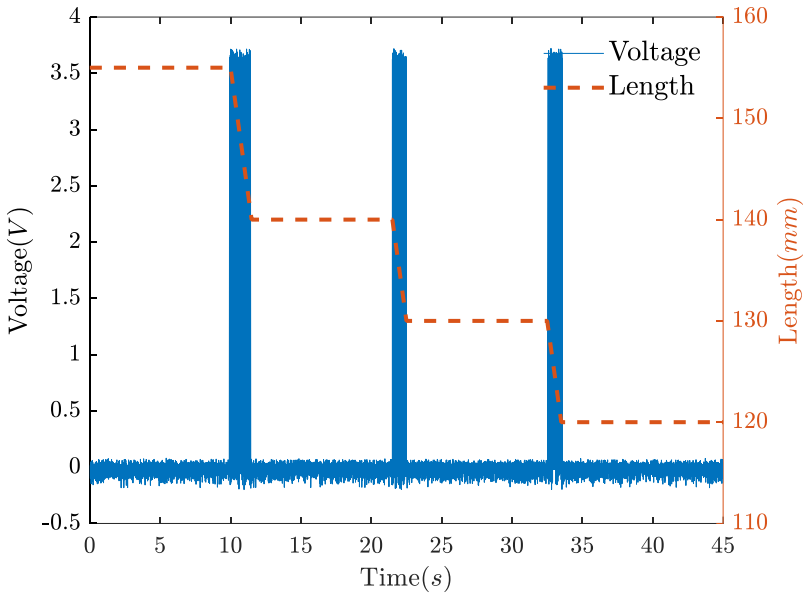

Fig. 14. Stepper motors PWM input and l-length change for the real-time l-length adjustment experiment.

It is depicted in Fig. 14 that the stepper motors varied the spring length over the time period of 45 seconds, using four different values with time intervals of 10s-11.5s, 21.5s-22.5s, and 32.5s-33.5s. The stepper motors took approximately 2 seconds to reach each desired length. The vibration responses of the mass and base were recorded and shown in Fig. 20. A recording time of 10 seconds was allocated prior to each movement of the stepper motors to reach the desired length, aiming to ensure the system stabilization.

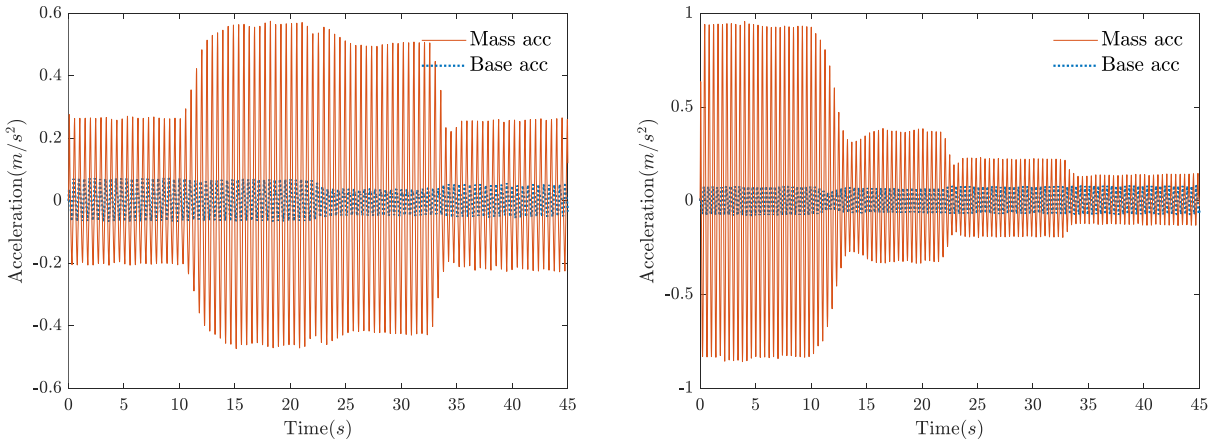

(a) (b)

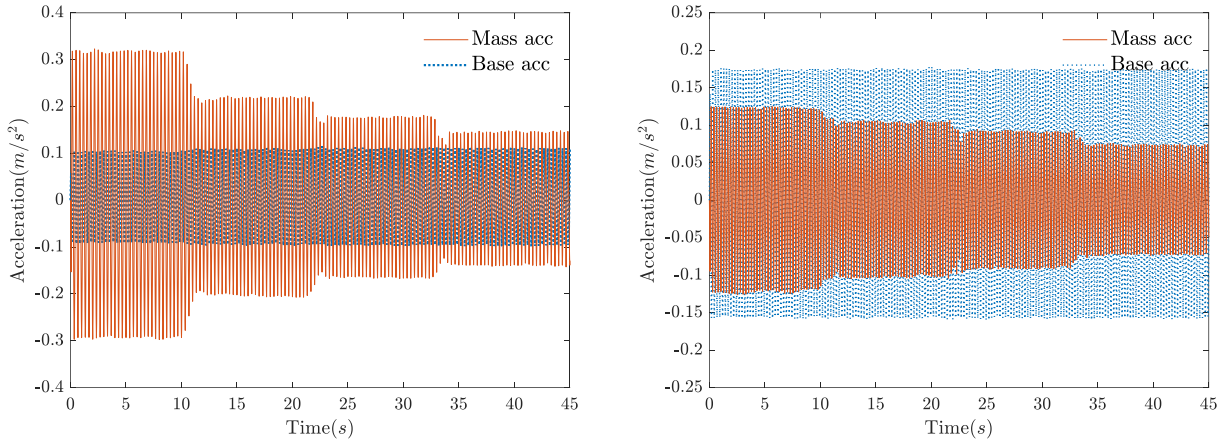

(c) (d)

Fig. 15. (a) Acceleration responses of the mass and base of the QZS system for the real-time l-length adjustment experiment with varying excitation frequencies: (a) ω=2.1 Hz, (b) ω =2.5 Hz, (c) ω =3 Hz, (d) ω =4 Hz.

As illustrated in Fig. 15, the real-time adjustment of the spring length l can effectively vary the transmissibility of the QZS system with sufficient high-responsiveness, demonstrating the feasibility of adaptive passive control strategy to quickly respond to changes in excitations. When the excitation frequency ω exceeded 2.1 Hz and the spring length was increased, the displacement transmissibility decreased as a consequence. At excitation frequencies of 3 Hz and 4 Hz, the change in displacement transmissibility was not obvious, as the suppressing of vibration was primarily governed by the inertia of the mass. However, the alteration in acceleration amplitude closely corresponds to the variation in the spring length, as depicted in Fig. 7.

6 Conclusions

This work proposed an adaptive passive control strategy aimed at improving the performance of a quasi-zero stiffness vibration isolator using controllable lateral springs. The system incorporated stepper motors mounted at both ends to adjust the nonlinear stiffness of the system, allowing the vibration isolation system to be regulated to avoid the excitation of large low-frequency resonance while improving the vibration control bandwidth. The work provided insights into how the vibration characteristics of the proposed QZS isolator can be regulated through the adaptive-passive control strategy with the goal of improving its vibration suppression performance. The key findings are as follows:

(a) The QZS vibration isolation system utilizes controllable variable-length lateral springs, with the system's stability and negative stiffness characteristics regulated by the adjustment of lateral spring length. The analysis shows that as the compression degree decreases, the system behaves more like a linear system. Considering that the system also exhibits non-linear characteristics, the stiffness ratio K of lateral and vertical springs should be increased accordingly when L increases. To prevent instability and maintain a single equilibrium point, it is crucial to ensure that the value of L remains below a specific line represented by $\gamma_1 = \sqrt{-4\alpha\gamma_2}$.

(b) To mitigate the large resonant response at low frequencies and optimize the control bandwidth, a displacement feedback control strategy is implemented, involving the active regulation of the length of lateral springs to dynamically alter the system stiffness. This approach exhibits high responsiveness, enabling it to quickly response to changes in external excitations so the system can switch its dynamic characteristic from a linear system to a nonlinear system and bypass the resonance. The proposed system owns the feature of an extended control bandwidth with low vibration transmissibility compared to the linear isolation system. The excitation of low-frequency resonance can be bypassed, while simultaneously decreasing the 0-dB transmissibility bandwidth so to improve the vibration isolation in the low frequency region.

(c) Experimental tests using stepper motors to manipulate lateral spring length demonstrated that the vibration isolation performance aligned well with theoretical predictions, showing the substantial reduction in vibration peaks due to its resonance compared to the non-controlled QZS system. The proposed system showcased 26.37% and 69.56% reduction in vibration peaks of the linear system and QZS system without control by varying the lateral spring stiffness based on the trigger frequency, along with a 11.81% increase in the vibration suppression bandwidth by reducing the 0-dB transmissibility bandwidth from 3.64 Hz to 3.21 Hz, compared to the linear vibration isolation system.

Acknowledgments

The authors acknowledge the support received from Ningbo Science and Technology Bureau - Ningbo Natural Science Foundation (project code 2022J176) China. This work was partially supported by the Nottingham Ningbo China Beacons of Excellence Research and Innovation Institute (budget code I01221100008) and the University of Nottingham Ningbo China – Li Dak Sum Innovation Scheme (budget code E06221200010).

References

[1] E. Rivin, Passive Vibration Isolation, Applied Mechanics Reviews. 57 (2004) B31–B32. https://doi.org/10.1115/1.1849173.

[2] R.A. Ibrahim, Recent advances in nonlinear passive vibration isolators, Journal of Sound and Vibration. 314 (2008) 371–452. https://doi.org/10.1016/j.jsv.2008.01.014.

[3] Z. Ma, R. Zhou, Q. Yang, Recent Advances in Quasi-Zero Stiffness Vibration Isolation Systems: An Overview and Future Possibilities, Machines. 10 (2022) 813. https://doi.org/10.3390/machines10090813.

[4] P.M. Alabuzhev, Vibration Protection And Measuring Systems With Quasi-Zero Stiffness, CRC Press, 1989.

[5] A. Carrella, M.J. Brennan, T.P. Waters, Static analysis of a passive vibration isolator with quasi-zero-stiffness characteristic, Journal of Sound and Vibration. 301 (2007) 678–689. https://doi.org/10.1016/j.jsv.2006.10.011.

[6] A. Carrella, M.J. Brennan, T.P. Waters, V. Lopes, Force and displacement transmissibility of a nonlinear isolator with high-static-low-dynamic-stiffness, International Journal of Mechanical Sciences. 55 (2012) 22–29. https://doi.org/10.1016/j.ijmecsci.2011.11.012.

[7] F. Zhao, J.C. Ji, K. Ye, Q. Luo, Increase of quasi-zero stiffness region using two pairs of oblique springs, Mechanical Systems and Signal Processing. 144 (2020) 106975. https://doi.org/10.1016/j.ymssp.2020.106975.

[8] F. Zhao, J. Ji, K. Ye, Q. Luo, An innovative quasi-zero stiffness isolator with three pairs of oblique springs, International Journal of Mechanical Sciences. 192 (2021) 106093–106093. https://doi.org/10.1016/j.ijmecsci.2020.106093.

[9] F. Zhao, J. Ji, Q. Luo, S. Cao, L. Chen, W. Du, An improved quasi-zero stiffness isolator with two pairs of oblique springs to increase isolation frequency band, Nonlinear Dynamics. 104 (2021) 349–365. https://doi.org/10.1007/s11071-021-06296-4.

[10] C. Liu, K. Yu, B. Liao, R. Hu, Enhanced vibration isolation performance of quasi-zero-stiffness isolator by introducing tunable nonlinear inerter, Communications in Nonlinear Science and Numerical Simulation. 95 (2021) 105654. https://doi.org/10.1016/j.cnsns.2020.105654.

[11] T.D. Le, K.K. Ahn, A vibration isolation system in low frequency excitation region using negative stiffness structure for vehicle seat, Journal of Sound and Vibration. 330 (2011) 6311–6335. https://doi.org/10.1016/j.jsv.2011.07.039.

[12] T.D. Le, K.K. Ahn, Experimental investigation of a vibration isolation system using negative stiffness structure, International Journal of Mechanical Sciences. 70 (2013) 99–112. https://doi.org/10.1016/j.ijmecsci.2013.02.009.

[13] Y. Wang, S. Li, S.A. Neild, Jason Zheng Jiang, Comparison of the dynamic performance of nonlinear one and two degree-of-freedom vibration isolators with quasi-zero stiffness, Nonlinear Dynamics. 88 (2017) 635–654. https://doi.org/10.1007/s11071-016-3266-3.

[14] C. Liu, K. Yu, Superharmonic resonance of the quasi-zero-stiffness vibration isolator and its effect on the isolation performance, Nonlinear Dynamics. 100 (2020) 95–117. https://doi.org/10.1007/s11071-020-05509-6.

[15] K. Ye, J.C. Ji, An origami inspired quasi-zero stiffness vibration isolator using a novel truss-spring based stack Miura-ori structure, Mechanical Systems and Signal Processing. 165 (2022) 108383. https://doi.org/10.1016/j.ymssp.2021.108383.

[16] H. Han, V. Sorokin, L. Tang, D. Cao, A nonlinear vibration isolator with quasi-zero-stiffness inspired by Miura-origami tube, Nonlinear Dynamics. 105 (2021) 1313–1325. https://doi.org/10.1007/s11071-021-06650-6.

[17] X. Yang, J. Zheng, J. Xu, W. Li, Y. Wang, M. Fan, Structural Design and Isolation Characteristic Analysis of New Quasi-Zero-Stiffness, Journal of Vibration Engineering & Technologies. 8 (2018) 47–58. https://doi.org/10.1007/s42417-018-0056-x.

[18] Z. Wu, X. Jing, J. Bian, F. Li, R. Allen, Vibration isolation by exploring bio-inspired structural nonlinearity, Bioinspiration & Biomimetics. 10 (2015) 056015. https://doi.org/10.1088/1748-3190/10/5/056015.

[19] H. Dai, X. Jing, Y. Wang, X. Yue, J. Yuan, Post-capture vibration suppression of spacecraft via a bio-inspired isolation system, Mechanical Systems and Signal Processing. 105 (2018) 214–240. https://doi.org/10.1016/j.ymssp.2017.12.015.

[20] X. Feng, X. Jing, Human body inspired vibration isolation: Beneficial nonlinear stiffness, nonlinear damping & nonlinear inertia, Mechanical Systems and Signal Processing. 117 (2019) 786–812. https://doi.org/10.1016/j.ymssp.2018.08.040.

[21] X. Liu, X. Huang, H. Hua, On the characteristics of a quasi-zero stiffness isolator using Euler buckled beam as negative stiffness corrector, Journal of Sound and Vibration. 332 (2013) 3359–3376. https://doi.org/10.1016/j.jsv.2012.10.037.

[22] X. Liu, Q. Zhao, Z. Zhang, X. Zhou, An experiment investigation on the effect of Coulomb friction on the displacement transmissibility of a quasi-zero stiffness isolator, Journal of Mechanical Science and Technology. 33 (2019) 121–127. https://doi.org/10.1007/s12206-018-1212-7.

[23] Y. Zheng, X. Zhang, Y. Luo, B. Yan, C. Ma, Design and experiment of a high-static–low-dynamic stiffness isolator using a negative stiffness magnetic spring, Journal of Sound and Vibration. 360 (2016) 31–52. https://doi.org/10.1016/j.jsv.2015.09.019.

[24] J. Xu, X. Yang, W. Li, J. Zheng, Y. Wang, M. Fan, W. Zhou, Y. Lu, Design of quasi-zero stiffness joint actuator and research on vibration isolation performance, Journal of Sound and Vibration. 479 (2020) 115367. https://doi.org/10.1016/j.jsv.2020.115367.

[25] D. Xu, Q. Yu, J. Zhou, S.R. Bishop, Theoretical and experimental analyses of a nonlinear magnetic vibration isolator with quasi-zero-stiffness characteristic, Journal of Sound and Vibration. 332 (2013) 3377–3389. https://doi.org/10.1016/j.jsv.2013.01.034.

[26] Wen Li Wu, X. Chen, Y. Shan, Analysis and experiment of a vibration isolator using a novel magnetic spring with negative stiffness, Journal of Sound and Vibration. 333 (2014) 2958–2970. https://doi.org/10.1016/j.jsv.2014.02.009.

[27] C. Liu, R. Zhao, K. Yu, B. Liao, In-plane quasi-zero-stiffness vibration isolator using magnetic interaction and cables: Theoretical and experimental study, Applied Mathematical Modelling. 96 (2021) 497–522. https://doi.org/10.1016/j.apm.2021.03.035.

[28] L.T. Danh, K.K. Ahn, Active pneumatic vibration isolation system using negative stiffness structures for a vehicle seat, Journal of Sound and Vibration. 333 (2014) 1245–1268. https://doi.org/10.1016/j.jsv.2013.10.027.

[29] X. Sun, J. Xu, X. Jing, L. Cheng, Beneficial performance of a quasi-zero-stiffness vibration isolator with time-delayed active control, International Journal of Mechanical Sciences. 82 (2014) 32–40. https://doi.org/10.1016/j.ijmecsci.2014.03.002.

[30] H. Pu, S. Yuan, Y. Peng, K. Meng, J. Zhao, R. Xie, Y. Huang, Y. Sun, Y. Yang, S. Xie, J. Luo, X. Chen, Multi-layer electromagnetic spring with tunable negative stiffness for semi-active vibration isolation, Mechanical Systems and Signal Processing. 121 (2019) 942–960. https://doi.org/10.1016/j.ymssp.2018.12.028.

[31] N. Zhou, K. Liu, A tunable high-static–low-dynamic stiffness vibration isolator, Journal of Sound and Vibration. 329 (2010) 1254–1273. https://doi.org/10.1016/j.jsv.2009.11.001.

[32] E. Palomares, A.J. Nieto, A.L. Morales, J.M. Chicharro, P. Pintado, Numerical and experimental analysis of a vibration isolator equipped with a negative stiffness system, Journal of Sound and Vibration. 414 (2018) 31–42. https://doi.org/10.1016/j.jsv.2017.11.006.

[33] G. Wen, J. He, J. Liu, Y. Lin, Design, analysis and semi-active control of a quasi-zero stiffness vibration isolation system with six oblique springs, Nonlinear Dynamics. 106 (2021) 309–321. https://doi.org/10.1007/s11071-021-06835-z.
[34] Y. Xiong, F. Li, Y. Wang, A nonlinear quasi-zero-stiffness vibration isolation system with additional X-shaped structure: Theory and experiment, Mechanical Systems and Signal Processing. 177 109208 (2022). https://doi.org/10.1016/j.ymssp.2022.109208.
[35] C. Liu, K. Yu, Design and experimental study of a quasi-zero-stiffness vibration isolator incorporating transverse groove springs, Archives of Civil and Mechanical Engineering. 20 (2020). https://doi.org/10.1007/s43452-020-00069-3.